Time Study of DNA Condensate Morphology: Implications Regarding the Nucleation, Growth, and Equilibrium Populations of Toroids and Rods†

Igor D. Vilfan, Christine C. Conwell, Tumpa Sarkar, and Nicholas V. Hud*

School of Chemistry and Biochemistry, Parker H. Petit Institute of Bioengineering and Biosciences, Georgia Institute of Technology, Atlanta, Georgia 30332-0400

Received February 27, 2006; Revised Manuscript Received April 28, 2006

ABSTRACT: It is well known that multivalent cations cause free DNA in solution to condense into nanometer-scale particles with toroidal and rod-like morphologies. However, it has not been shown to what degree kinetic factors (e.g., condensate nucleation) versus thermodynamic factors (e.g., DNA bending energy) determine experimentally observed relative populations of toroids and rods. It is also not clear how multimolecular DNA toroids and rods interconvert in solution. We have conducted a series of condensation studies in which DNA condensate morphology statistics were measured as a function of time and DNA structure. Here, we show that in a typical in vitro DNA condensation reaction, the relative rod population 2 min after the initiation of condensation is substantially greater than that measured after morphological equilibrium is reached (ca. 20 min). This higher population of rods at earlier time points is consistent with theoretical studies that have suggested a favorable kinetic pathway for rod nucleation. By using static DNA loops to alter the kinetics and thermodynamics of condensation, we further demonstrate that reported increases in rod populations associated with decreasing DNA length are primarily due to a change in the thermodynamics of DNA condensation, rather than a change in the kinetics of condensate nucleation or growth. The results presented also reveal that the redistribution of DNA from rods to toroids is mediated through the exchange of DNA strands with solution.

Upon association with multivalent cations, DNA condenses from its extended state in solution into nanometer-scale particles (*1*−*4*). This phenomenon has been studied by biophysicists for over thirty years (*5*−*15*), often as a model of DNA packaging within viruses and sperm cells. Polymer physicists have also used DNA condensation as a model system to study the general behavior of polyelectrolytes in the presence of multivalent counterions (*16*−*26*). From a more applied perspective, understanding the factors that govern the size and shape of DNA condensates is believed to be important for the optimization of artificial gene delivery (*27*, *28*).

The particles formed when DNA is condensed in vitro can vary significantly in size (i.e., ∼50−300 nm) and morphology (e.g., toroids, rods, and spheres). Both of these characteristics can depend on solution conditions (e.g., ionic strength and solvent polarity) (*29*−*31*), DNA properties (e.g., length, persistence length, and extent of supercoiling) (*31*−*34*), and the nature of the condensing agent (e.g., charge density) (*35*, *36*). DNA condensate formation has been shown to be a nucleation−growth phenomenon (*1*, *11*, *30*−*32*, *37*−*39*). For example, the first step of toroid formation is the spontaneous appearance of a nucleation loop, which is followed by the intramolecular collapse of the DNA polymer to form a monomolecular proto-toroid (*31*, *38*). The proto-toroid then grows larger by collecting additional DNA molecules from the solution (*30*, *31*). The nucleation and growth of DNA condensates with alternative morphologies (e.g., rods and spheres) has also been studied experimentally (*35*, *36*) but is not as well characterized.

Most theoretical studies of DNA condensation have focused on the earliest stages of particle formation and have almost exclusively modeled monomolecular condensation (*25*, *26*, *40*−*44*). Some computer simulations have suggested that a monomolecular rod represents a metastable state, which converts to the more thermodynamically stable toroid by internal conversion or by complete decondensation followed by recondensation into a toroid (*25*, *26*, *40*, *41*, *43*, *44*). Experimentally observed nonequilibrium distributions of rods and toroids should, therefore, be expected to depend on the probability for rod and toroid nucleation as well as the rate of conversion of rods to toroids. However, it has also been proposed that the packing of DNA in rods and toroids is virtually isoenergetic (*1*), suggesting that these two morphologies could coexist in a Boltzmann distribution at equilibrium. It is, therefore, possible that the observed distributions of toroids and rods actually depend on both the thermodynamics and kinetics of DNA condensate formation. With regard to particle growth, theoretical models that have addressed multimolecular condensation do in fact predict that particle growth should be sensitive to both kinetic and thermodynamic factors (*45*). Thus, if we are to completely understand the phenomenon of DNA condensation, it is important to experimentally characterize the mechanisms by which multimolecular DNA condensates change in morphology and size over time.

† This work was supported by research grant GM62873 from the National Institutes of Health.

* To whom correspondence should be addressed. Tel: 404-385-1162. Fax: 404-894-7452. Email: hud@chemistry.gatech.edu.

10.1021/bi060396c CCC: $33.50
Published on Web 06/08/2006

Analyses of DNA condensate size and morphology as a function of one or more independent variables have proven very useful for testing hypotheses regarding the phenomenon of DNA condensation. For example, the measurements of toroid dimensions for DNA condensed in different ionic strength buffers have revealed that the size of condensates produced under typical laboratory conditions is determined by the kinetics of condensation rather than thermodynamic growth limits (*30*). Here, we report the analysis of particles formed by DNA and hexammine cobalt chloride as a function of time for the first 3 h after the initiation of condensation. Using transmission electron microscopy (TEM), we have observed a gradual decrease in relative rod populations and a corresponding increase in relative toroid populations. These relative populations stabilize within approximately 20 min. Our observation that relative toroid and rod populations are not initially at their equilibrium values indicates that condensate morphology can be governed, in part, by the nonequilibrium process of condensate nucleation. The time required to reach morphological equilibrium is shown to decrease, if the ionic strength of the condensation reaction is increased; however, the relative populations of rods and toroids remains the same at equilibrium.

In addition to the observed shift in morphology, DNA condensates were observed to continuously grow in size for at least 3 h after the initiation of condensation, which is in agreement with previously reported data (*46*). Under low ionic strength conditions, changes in condensate morphology populations and size are not temporally correlated. Rather, relative toroid and rod populations reach their equilibrium values before appreciable condensate growth is detected by TEM. The rate of condensate growth is also shown to increase with the ionic strength of the condensation reaction. Here, we also demonstrate that DNA length and the introduction of static loops can significantly alter the initial and equilibrium populations of rods and toroids. The results of this study reveal that both kinetic and thermodynamic factors govern observed populations of rods and toroids. The results presented are used to develop a unified model for multimolecular DNA condensate formation, morphology interconversion, growth, and approach to equilibrium.

EXPERIMENTAL PROCEDURES

DNA Preparation. Plasmid DNA (2961 bp) Bluescript II SK− (Stratagene, La Jolla, CA) was grown in DH5α cells (Life Technologies, Rockville, MD) and isolated using the Qiagen Maxi Prep kit (Qiagen, Valencia, CA). DNA was dissolved in 1× TE (10 mM Tris at pH 7.8, 1 mM EDTA) in the final step of isolation. The purified Bluescript II SK− plasmid DNA was linearized by digestion with the restriction enzyme *Hin*dIII (New England Biolabs, Beverly, MA). The linearized Bluescript II SK− plasmid DNA is referred to as *3kbDNA* throughout the text. A Bluescript II SK− plasmid was previously modified by the insertion of two tandem repeats of the multiple-phased A-tract sequence 5′-ATCCATCGACC($A_6CG_3CA_6CG_2C$)$_7$$A_6$GCAGTGGAAG-3′, which produces approximately one full loop of sequence-directed curvature (*38*). This plasmid was grown in Sure2 Supercompetent cells (Stratagene), isolated as described above, and linearized with *Hin*dIII and is referred to as *3kbAtract*.

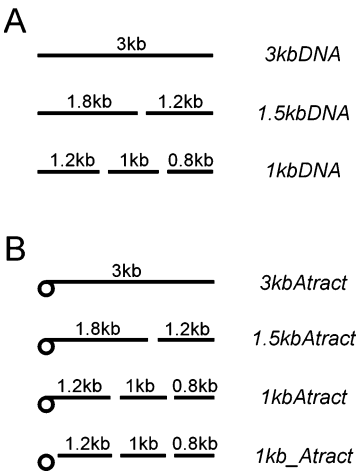

FIGURE 1: Schematic representation of the DNA samples used in the present study. For each sample, the molar concentrations of all DNA fragments are identical. The abbreviated name for each sample represents the average length of DNA fragments in the sample. The procedure used to generate each sample is described in Experimental Procedures.

To obtain shorter DNA fragment lengths, samples of *3kbDNA* and *3kbAtract* were digested with additional restriction enzymes (Figure 1). *3kbDNA* was digested with *Sca*I (New England Biolabs) to yield a mixture of 1.2 and 1.8 kb fragments (referred to as *1.5kbDNA* to reflect the average fragment length in the sample). *3kbDNA* was digested with *BspH*I (New England Biolabs) to obtain a mixture of 0.8, 1.0, and 1.2 kb fragments (referred to as *1kbDNA*). *3kbAtract* was digested with *Sca*I to yield a mixture of 1.2 and 1.8 kb fragments, with the A-tract loop located at one end of the 1.8 kb fragment (sample referred to as *1.5kbAtract*). *3kbAtract* was digested with *BspH*I to obtain a mixture of 0.8, 1.0, and 1.2 kb fragments, with the A-tract loop located at one end of the 1.2 kb fragment (sample referred to as *1kbAtract*). *3kbAtract* was double digested with *BspH*I and *Xba*I (New England Biolabs) to obtain a mixture of 0.8, 1.0, and 1.2 kb fragments and the 0.4 kb A-tract loop (sample referred to as *1kb_Atract*). The restriction enzyme buffers were removed from all DNA samples after digestion by rinsing at least five times with 1× TE using a Microcon YM-30 spin column (Amicon, Billerica, MA). After the final rinse, DNA samples were eluted with 1× TE to yield stock solutions. NaCl in 1× TE buffer was added to a fraction of each DNA sample stock solution to obtain stock solutions in a higher ionic strength buffer (10 mM Tris, 7.5 mM NaCl at pH 7.8, 1 mM EDTA). All DNA samples were diluted from stock solutions to 20 μg/mL in their respective buffers. DNA concentrations were confirmed spectrophotometrically on the basis of the absorbance at 260 nm.

Preparation of Condensation Solutions and EM Grids. For all DNA samples, DNA condensation reactions were initiated by mixing equal-volume solutions of DNA and hexammine cobalt chloride (Sigma) to yield reaction mixtures: 10 μg/mL in DNA, 100 μM in hexammine cobalt chloride, and 0.5× in the respective buffer of the DNA sample. Each DNA condensate reaction was then allowed to incubate in the reaction tube at room temperature. The aliquots (5 μL) of each condensation reaction were removed from the reaction tube at different incubation times (from less than 1 min to 3 h) and deposited on carbon-coated grids

(Ted Pella, Redding, CA). After 10 min of incubation on the grid, an equal volume of 2% uranyl acetate (Ted Pella) was added to the condensate mixture. After 1 min of uranyl acetate staining, the grids were rinsed in 95% ethanol and air-dried. The reaction time for each DNA condensation reaction was calculated by summing the incubation time in the reaction tube, the incubation time on the grid, and the staining time. To prepare DNA condensates with total condensation times shorter than 11 min, the condensation reaction mixtures were prepared as described above and then immediately deposited on grids for varying incubation times (1 to 10 min), after which an equal volume of 2% uranyl acetate was added. After 1 min of uranyl acetate staining, the grids were rinsed in 95% ethanol and air-dried. The DNA condensation time for this set of experiments was calculated by summing the incubation time on the grid and the staining time.

Analysis of DNA Condensate Morphology and Size. All grids were examined with a JEOL-100C transmission electron microscope (TEM). The relative toroid and rod populations in each sample were determined by counting the number of unclustered toroids and rods. At least 500 DNA condensates were counted for each sample. As mentioned above, the imaging of DNA condensates for reaction times shorter than 11 min required shorter sample incubation times on the EM grids. To confirm that varying the incubation time of a sample on a grid did not bias morphology population statistics a control study with *3kbDNA* was performed with various condensation times in the reaction tube but with a uniform grid incubation time of 1 min. The relative toroid and rod populations measured were identical, within error, to those measured using grid incubation times of 11 min (data not shown). TEM images of DNA condensates were recorded on film at 100 000× magnification. TEM negatives were scanned at 300 dpi into an electronic format, and a graphics program was used to measure the size of individual toroids and rods in each sample.

Determination of Free DNA Concentration. The amount of uncondensed DNA (i.e., free DNA) present from 2 min to 3 h after the initiation of condensation was measured using a combination of two techniques, differential ultracentrifugation (*46*) and circular dichroism (CD) (*47*), previously established for quantifying the extent to which DNA is condensed in solution. For these experiments, 750 μL of 20 μg/mL of DNA was condensed by mixing with an equal volume of 200 μM hexammine cobalt chloride in the buffer conditions described above. The DNA in this mixture was allowed to condense for different reaction times in centrifuge tubes, followed by the sedimentation of condensed DNA using a Beckman Coulter Optima Ultracentrifuge with a TLS 55 rotor operated at 55 000 rpm (259000*g*) for 20 min at 20 °C. After sedimentation, 70 μL of each supernatant was taken at the meniscus, and the DNA concentration was determined on the basis of A_{260}. A control solution of uncondensed DNA (10 μg/mL) in the same buffer confirmed that free DNA does not detectably sediment when subjected to the same centrifugation conditions. These studies revealed that within 21 min after the initiation of condensation <10% of the DNA is uncondensed, and this amount remains constant for at least 3 h (Supporting Information, Figure S1). It was not possible to measure the amount of free DNA present at shorter condensation times by differential centrifugation because of the time required to sediment DNA condensates. However, the CD spectrum of a condensed DNA sample measured 2 min after the initiation of condensation was indistinguishable from spectra collected from 2 to 72 min, indicating that within 2 min DNA is condensed to the same extent that it is at later times for which the free DNA concentration was determined by differential centrifugation (Supporting Information, Figure S2).

RESULTS AND DISCUSSION

To determine whether the kinetics of condensate nucleation influences the observed relative populations of toroids and rods, we have performed studies of DNA condensate morphology as a function of time. The DNA condensates were prepared throughout this study using hexammine cobalt chloride as a condensing agent. For a range of experimental conditions, hexammine cobalt chloride and other multivalent cations have been shown to condense DNA into toroids and rods, with other morphologies representing only a minor fraction of the condensate population (*1*, *33*, *48*−*50*). Consistent with previous studies, toroids and rods were observed to be the two most prevalent morphologies for all samples analyzed, with other condensate morphologies accounting for less than 1% of the total population. Unless otherwise stated, all morphology statistics presented were obtained by counting only individual (i.e., not aggregated) toroids and rods.

Rod Populations Are Initially Greater than at Equilibrium. Linear 2961 bp plasmid DNA, referred to as *3kbDNA* (Figure 1), was condensed at room temperature with hexammine cobalt chloride in a low ionic strength buffer (5 mM Tris at pH 7.8, 0.5 mM EDTA), with final DNA and hexammine cobalt chloride concentrations of 10 μg/mL and 100 μM, respectively. The DNA condensate morphologies present at different reaction times were determined using transmission electron microscopy (TEM) (Experimental Procedures). Two minutes after the initiation of the condensation reaction, both toroids and rods were observed (Figure 2A), accounting for 79% and 21% of all individual condensates, respectively. When the condensation reaction time was increased to 16 min, the relative population of toroids increased (Figure 2B), with toroids representing 87% and rods 13% of all condensates (Figure 3). Increasing the condensation reaction time to 41 and 71 min resulted in both samples containing 97% toroids and only 3% rods (Figures 2C and 3). These relative toroid and rod populations remained unchanged after a 3 h condensation time. On the basis of an estimated time constant for the morphology conversion of approximately 15 min (Figure 3), the relative populations of 97% toroids and 3% rods observed between 41 min and 3 h apparently represent equilibrium populations for a sample of *3kbDNA* condensed by hexammine cobalt chloride under low ionic strength conditions.

For condensation times longer than 41 min, clusters of toroids and rods, and morphologically less defined aggregates, were observed with significantly greater frequency compared to that of samples examined at shorter condensation times (Figure 2). An investigation of relative toroid and rod populations within condensate clusters in a sample of condensed *3kbDNA* also revealed a steady decrease in relative rod populations. For example, after 2 min of

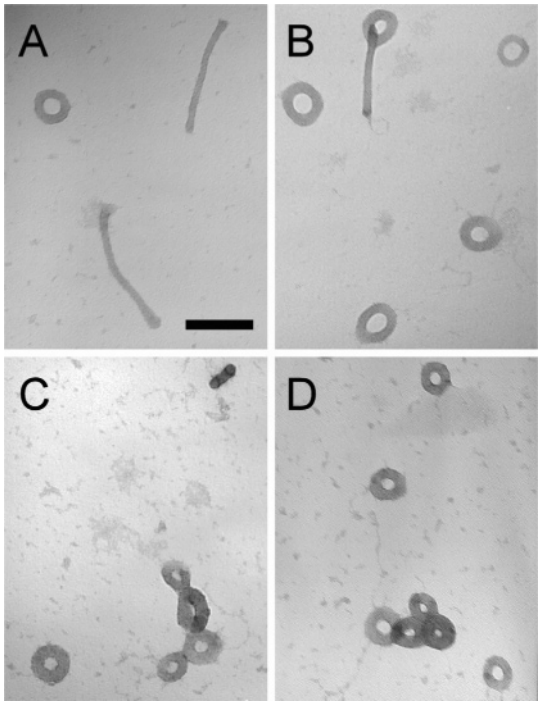

FIGURE 2: Transmission electron micrographs of DNA condensates at different times after the mixing of *3kbDNA* and hexammine cobalt chloride in the low ionic strength buffer. (A) 2 min after the initiation of condensation; (B) 16 min after the initiation of condensation; (C) 41 min after initiation of condensation; (D) 71 min after initiation of condensation. Additional experimental details are provided in Experimental Procedures. The scale bar in A is 100 nm. The magnification is the same for all images.

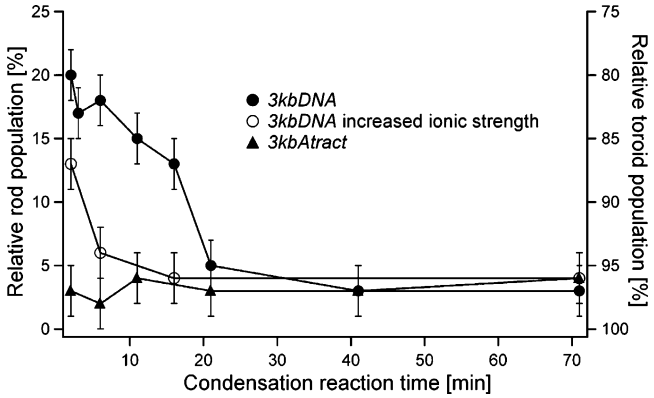

FIGURE 3: Relative rod and toroid populations as a function of time for three samples with the DNA approximately 3 kb in length. Samples *3kbDNA* and *3kbAtract* were condensed with hexammine cobalt chloride in the low ionic strength buffer. The data designated as *3kbDNA* increased ionic strength corresponds to *3kbDNA* condensed with hexammine cobalt chloride in the higher ionic strength buffer. Buffer definitions and additional experimental details are provided in Experimental Procedures. The uncertainty indicated in relative toroid and rod population measurements was estimated by repeatedly counting (three times) the number of unclustered toroids and rods for one sample of condensed *3kbDNA*.

condensation time, the rods represented 10% of all clustered DNA condensates, whereas after 71 min, the rods accounted for only 2% of all clustered particles. Thus, the observed change in the relative populations of individual toroids and rods cannot be attributed to the preferential aggregation of rods.

The observed changes in relative toroid and rod populations demonstrate that rod populations are kinetically biased during earlier stages of DNA condensation compared to that of their equilibrium populations. This observation provides experimental support for polymer simulations, which have suggested that toroids are more thermodynamically stable than rods but that rods may appear in greater numbers than dictated by the Boltzmann distribution because of the favorable kinetics of nucleation (*25*, *26*, *40*−*44*, *51*−*56*). Nevertheless, rods do not completely disappear from *3kbDNA* condensation mixtures even hours after significant changes in morphology populations are no longer detected, indicating that rods represent a thermodynamically accessible state for condensed DNA at room temperature.

Rod Populations Decrease over Time through the Redistribution of DNA Strands. The observed decrease in relative rod populations with time suggests a decrease in absolute rod concentration. However, an increase in absolute toroid concentration could also produce the observed decrease in relative rod population. Condensate populations determined by counting toroids and rods on EM grids does not provide information regarding the absolute number of DNA condensates present in a solution. An increase in absolute toroid concentration over time could, in theory, result from the formation of new toroids from the free (i.e., uncondensed) DNA still present in the solution minutes after the initiation of condensation. To evaluate this possibility, we used differential ultracentrifugation and CD spectroscopy to measure the concentration of free DNA in condensation reaction mixtures as a function of time (Experimental Procedures). The amount of free DNA present 2 min after the initiation of condensation was determined to be <10%, a value that remained constant over the time period when changes in relative toroid and rod populations were observed. Thus, the equilibrium between free and condensed DNA is established before the equilibrium between rods and toroids is reached. We are, therefore, able to eliminate the possibility that the observed decrease in relative rod population with time is due to the formation of new toroids from previously uncondensed DNA.

One might also argue that the observed decrease in relative rod populations could result from the dissociation of toroids over time into a greater number of smaller toroids. If we assume a constant absolute rod concentration, then each toroid observed at a reaction time of 2 min would have to yield approximately eight toroids when the equilibrium population had been reached. Such a redistribution of DNA would result in a decrease in average toroid thickness by a factor of approximately 3. However, mean toroid thickness, which was measured to be 22 nm at 2 min after condensation initiation, was observed to increase over time, not decrease (Figure 4A and Supporting Information, Figure S3).

On the basis of the results and arguments presented above, we can conclude that the observed decrease in relative rod populations over time is in fact due to a decrease in the absolute concentration of rods. However, it is not self-evident by what mechanism the DNA initially condensed into rods becomes condensed into toroids. It has been previously recognized that the mean thickness of DNA toroids is essentially equal to the mean thickness of DNA rods, and the mean circumference of toroids is essentially equal to the mean length of rods (*33*, *35*, *57*, *58*). This observation has been used to support a model for toroid formation in which rods convert into toroids by bending and end fusion (*58*).

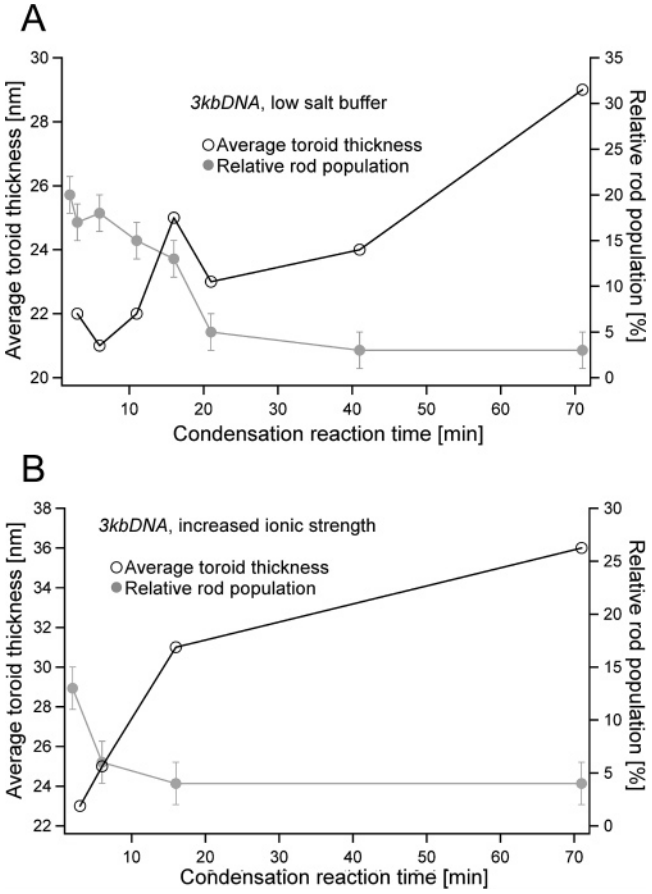

FIGURE 4: Plots of average toroid thickness as a function of time for (A) (○) *3kbDNA* condensed in the low ionic strength buffer and (B) (○) *3kbDNA* condensed in the higher ionic strength buffer. For comparison, the relative rod populations (●) are also shown for each sample. The experimental details are provided in Experimental Procedures.

However, we did not observe features in the TEM images of toroids that would suggest regions where the ends of a rod had fused. An alternative explanation for the shift of condensed DNA from rods to toroids is the decondensation of DNA from rods to an extent that most rods completely disintegrate within the first few minutes after the initiation of condensation (Figure 3). The DNA released from rods would only be transiently free in solution before recondensing onto existing toroids and remaining rods or nucleating new condensates.

If the DNA released from rods predominately nucleated new condensates, then the size of toroids within the condensation reaction would not increase with time. In contrast, if the DNA released from the existing rods and toroids primarily recondensed onto preexisting condensates, then an increase in average condensate size would be expected over time. Most of the observed decrease in the rod population for *3kbDNA* (from approximately 20% to 5%) occurs within the first 21 min after the initiation of condensation (Figure 3). During this same time period, the observed increase in toroid thickness is not statistically significant (Figure 4A). However, the lack of considerable growth by toroids between 2 and 21 min does not necessarily imply that the DNA released from the rods is not primarily recondensed onto the toroids. We note that even if all of the DNA lost from the rods between 2 and 21 min (representing 15% of all DNA) were recondensed onto the existing toroids, the mean thickness of the toroids would only increase by approximately 2 nm. As discussed in the following section, condensate growth over a longer time period provides definitive evidence that DNA is gradually redistributed among a decreasing number of condensates.

DNA Strand Redistribution as a Mechanism for Particle Growth. An analysis of DNA toroid dimensions revealed that the thickness of *3kbDNA* toroids increased appreciably between 2 min and 3 h after the initiation of condensation (Figure 4A and Supporting Information, Figure S3). For example, mean toroid thickness was measured to be 22 nm at 2 min, 29 nm at 71 min, and 32 nm at 3 h. The rods were also observed to increase in thickness over time. The mean rod thickness measured after 2 and 21 min was 18 and 20 nm, respectively. Because of the decrease in rod population to only 3% after 21 min, a mean rod thickness was not calculated for longer condensation times. However, TEM images revealed a qualitative increase in rod thickness similar to that observed for toroids (data not shown). The fact that toroids and rods continued to grow in thickness after a morphological equilibrium had been reached (i.e., after 21 min) indicates that DNA strand redistribution among existing condensates and the complete decondensation of some condensates must occur for both toroids and rods for several hours. Thus, the relative population of rods and toroids in a sample reaches its equilibrium value long before the particles in the same sample reach their thermodynamically favored size, if this size is ever reached.

The results presented above demonstrate that the process of DNA condensation by hexammine cobalt chloride can be subdivided into three stages that take place on different time scales. The first stage, the initial condensation of DNA, establishes an equilibrium state of condensed and free DNA. This stage has been previously shown to be complete within the millisecond time frame (*59*, *60*) and includes proto-toroid/proto-rod formation (i.e., nucleation and intramolecular condensation) as well as initial particle growth by the addition of previously uncondensed DNA. The second stage includes the shift in condensate morphology to relatively more toroids and fewer rods as well as continued particle growth. In the present study, the rod-toroid morphological equilibrium was reached on the minute time scale. The aggregation of individual condensates can be considered as the third and final stage, which occurs on a time frame of hours to days. These three stages have been incorporated into the overall model of DNA condensation presented schematically in Figure 5. A constant equilibrium concentration of free DNA is proposed to provide the conduit for the transition to morphological equilibrium (Figure 5). Similarly, condensate strand exchange between preexisting condensates occurs through DNA exchange with solution (Figure 5). Under the conditions of the present study, the three stages described are temporally separated. However, changes in condensation conditions (e.g., DNA and condensing agent concentrations, DNA length, condensing agent structure, and ionic strength) can undoubtedly change the time scales of one or more of these stages and, thereby, change what is observed in the laboratory time frame as the overall condensation process. The effects of ionic strength, DNA length, and DNA structure on the observed equilibrium populations of rods and toroids and the rate of approach to this equilibrium is explored in the following sections.

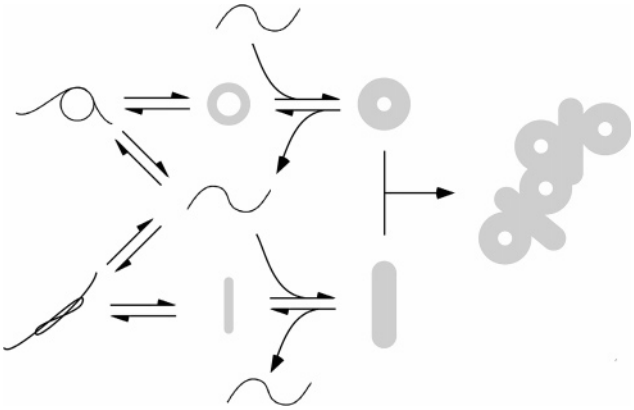

FIGURE 5: Model for the overall process of DNA condensation in which both rods and toroids are formed. DNA at different stages of condensation and DNA condensed into different morphologies are shown to be in exchange through the common intermediate of free DNA in solution. The three stages described in the text as being temporally separated in the present study are (left to right) (I) toroid/rod nucleation, the formation of monomolecular condensates by intramolecular condensation and initial particle growth; (II) continued particle growth and morphology interconversion through strand exchange with solution; and (III) the aggregation of rods and toroids.

NaCl Increases the Rate of DNA Strand Redistribution. The experiments described above were carried out in a low ionic strength buffer to maximize the observed effects of condensation kinetics on particle size and morphology because we have previously shown that condensate size is kinetically limited under low salt conditions (*30*, *31*). To investigate the effect of monovalent cation concentrations on DNA morphology conversion kinetics, toroid and rod populations were also examined for *3kbDNA* condensed in a buffer of slightly higher ionic strength (i.e., 3.75 mM NaCl, 5 mM Tris at pH 7.8, 0.5 mM EDTA). We note that condensation could not be carried out under significantly higher ionic strength conditions without also increasing the concentration of hexammine cobalt chloride because DNA condensation by this trivalent cation is completely prevented upon a sufficient increase in monovalent metal ion salts (*31*, *61*). As shown in Figure 3, the relative equilibrium populations of rods and toroids measured for condensed *3kbDNA* do not change appreciably with this increase in ionic strength. However, the time required for the condensates of *3kbDNA* to reach morphological equilibrium is shorter in the presence of a higher ionic strength buffer (ca. 10 min) (Figure 3).

The mean thickness of *3kbDNA* toroids was also observed to increase more rapidly in the higher ionic strength buffer (Supporting Information, Figure S4). For example, the mean toroid thickness for the low and higher ionic strength buffers were virtually identical 2 min after the initiation of condensation, measuring at 22 and 23 nm, respectively. However, the mean toroid thickness increased to 36 nm at 71 min in the higher ionic strength buffer compared to 29 nm for the low ionic strength buffer. A further differential increase in toroid dimensions was also observed at 3 h, with the mean toroid thickness increasing to 57 nm in the higher ionic strength buffer compared to 32 nm in the low ionic strength buffer (Supporting Information, Figures S3 and S4). Rods produced in the higher ionic strength buffer were observed to increase in thickness at a similar rate but not in length (data not shown).

Our measurements of *3kbDNA* condensates clearly demonstrate that the rate of attaining morphological equilibrium and the rate of toroid growth (i.e., thickness) both increased when the ionic strength of the condensation solution was increased (Figures 3 and 4). As mentioned above, monovalent cations decrease the propensity of the multivalent cations to condense DNA (*61*). Thus, at increased monovalent salt concentrations we expect a reduced association constant between DNA strands condensed by trivalent cations, which would be the result of a decrease in DNA strand association rate and/or an increase in DNA strand dissociation rate at equilibrium. Because the equilibrium between free and condensed DNA is reached within the first two minutes of the condensation reaction (under our experimental conditions), the observed higher rates of morphology conversion and condensate growth must be because of a more rapid exchange of DNA strands between the condensates after the initial condensation has taken place. These results are consistent with our proposal that the conversion of rods to toroids takes place through the exchange of DNA strands between the condensates and the solution.

Nucleation Advantage of Rods Can Be Eliminated by Static DNA Loops. We have previously demonstrated that one or more static DNA loops, in an otherwise linear DNA molecule, can act as built-in nucleation sites for toroidal condensates (*31*, *38*). A static loop within plasmid DNA was created by the introduction of multiple A-tract sequences (*62*, *63*). In our previous investigations, the reduced diameter of toroids formed by DNA molecules containing static loops was presented as evidence that static loops act as nucleation sites for toroids (*31*, *38*). Uniformly curved DNA duplexes constructed exclusively from phased A-tract sequences have also been shown to produce smaller toroids than those produced by the DNA without static curvature (*64*), which illustrates that the DNA bent by A-tracts is favorably accommodated into toroidal condensates. In the present study, we have investigated the effects of A-tract loops on nonequilibrium and equilibrium populations of toroids and rods produced by samples primarily DNA with no static curvature.

A 3.3 kb DNA plasmid containing A-tract sequence-directed curvature of approximately 360° over a 346 bp segment (i.e., a 37 nm diameter loop) was digested with a restriction enzyme (Experimental Procedures) such that the static loop was located near one end of the linearized plasmid (referred to as *3kbAtract*; Figure 1). *3kbAtract* was condensed in the low ionic strength buffer as described above. After 2 min of condensation time, the toroids accounted for 97% of all individual condensates, with rods representing the remaining 3%, which represents a considerable decrease in the relative rod population compared to that of *3kbDNA* at the same condensation time (Figure 3). An analysis of *3kbAtract* samples for up to 3 h after the initiation of condensation did not reveal a further decrease in the relative rod population. The lower initial rod population observed for *3kbAtract* confirms that static A-tract loops alter the condensation of 3 kb DNA, primarily by altering the kinetics of condensate nucleation. We note that equilibrium rod and toroid populations of *3kbAtract* (and all other DNA molecules in this study) did not change when prepared and measured in the higher ionic strength buffer (Figure 6).

Effect of DNA Length on Condensate Nucleation and Morphological Equilibrium. DNA that is shorter than 1.5

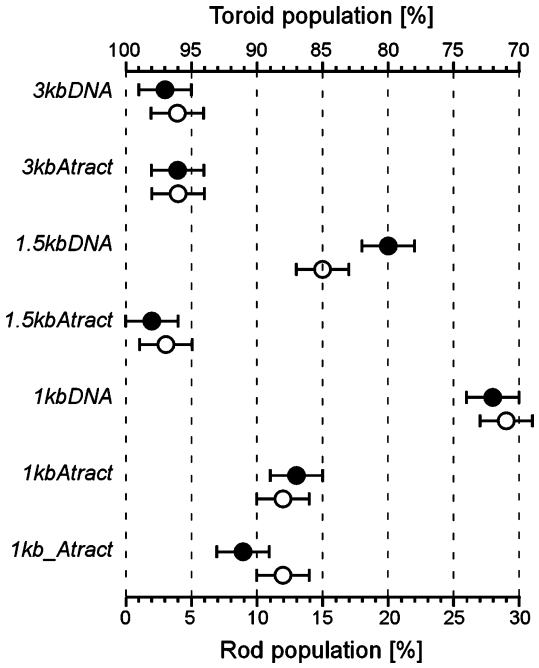

FIGURE 6: Comparison of the relative toroid and rod populations at morphological equilibrium for all DNA samples analyzed in the present study. All DNA samples were condensed with hexammine cobalt chloride in the low ionic strength (●) and the higher ionic strength (○) buffers as described in Experimental Procedures. The condensation mixtures were allowed to react for 71 min to reach morphological equilibrium. The error bars are estimated as described in Figure 3.

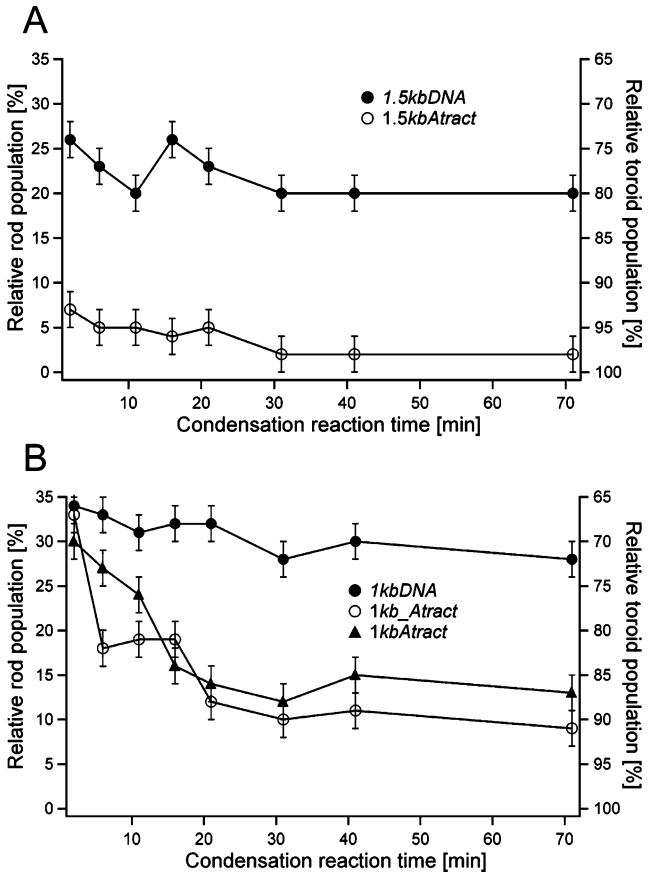

FIGURE 7: Time-dependent rod and toroid populations for DNA samples with average lengths of 1.5 and 1 kb. (A) Samples with average DNA fragment lengths of 1.5 kb. (B) Samples with average DNA fragment lengths of 1 kb. All DNA samples presented were prepared by condensing DNA with hexammine cobalt chloride in the low ionic strength buffer. The experimental details are provided in Experimental Procedures.

kb has previously been shown to produce a greater percentage of rods than longer DNA (*32*, *33*). To investigate the effect of DNA length on condensate morphology as a function of time and at equilibrium, condensation studies were performed using DNA samples with average fragment lengths of approximately 1.5 kb and 1 kb (Experimental Procedures). The sample referred to as *1.5kbDNA* contained an equimolar mixture of two fragments, 1.2 and 1.8 kb in length. The sample referred to as *1kbDNA* contained an equimolar mixture of three fragments, 0.8, 1.0, and 1.2 kb in length (Figure 1).

Samples *1.5kbDNA* and *1kbDNA* were condensed in the low ionic strength buffer as described above. The relative rod populations for both *1.5kbDNA* and *1kbDNA* were greater than those observed for the *3kbDNA* sample at all time points measured (Figures 3 and 7). The relative rod populations at 2 min for condensed *1.5kbDNA* and *1kbDNA* were 26% and 34%, respectively. These values are 6% and 15% greater than the 2 min rod population measured for *3kbDNA*. The relative rod populations of *1.5kbDNA* and *1kbDNA* were also observed to decrease over time (Figure 7). However, the changes in these populations were less pronounced compared to that of *3kbDNA* (Figures 3 and 7). The relative rod populations of *1.5kbDNA* and *1kbDNA* each decreased by only 5% from their 2 min populations to reach their equilibrium populations of 20% and 28%, respectively. In contrast, the *3kbDNA* sample decreased more than 15% from an initial rod population of 20% to 3% at equilibrium.

The greater equilibrium rod population of *1.5kbDNA* compared to that of *3kbDNA* demonstrates that reducing DNA length from 3 to 1.5 kb has a significant effect on the relative thermodynamic stability of rods and toroids. The additional increase in equilibrium rod population associated with reducing average DNA fragment length from 1.5 to 1 kb (i.e., 20% vs 28%) provides further support for this relationship between DNA length and the relative stability of rods and toroids (Figure 7).

The smaller difference between the initial rod populations of *1.5kbDNA* and *3kbDNA* (ca. 5%) compared to the difference in their equilibrium rod populations (ca. 17%) suggests that initial (i.e., kinetically biased) rod populations are affected to a lesser degree when DNA length is shortened from 3 to 1.5 kb. The smaller difference observed between the rod populations at 2 min versus the equilibrium populations could also be indicative of a more rapid approach to morphological equilibrium by the *1.5kbDNA* sample. However, this does not appear to be the case because the results described in the following sections indicate that morphological equilibrium for samples containing average DNA lengths of 1.5 and 1 kb in the presence of static A-tract loops (i.e., *1.5kbAtract* and *1kbAtract*, vide infra) takes place with a similar time constant.

Static Loops Shift the Morphological Equilibrium of Shorter DNA Fragments. To further characterize the observed increase in relative rod populations for DNA samples with decreasing length both as a function of time and at equilibrium, we studied the condensation of DNA fragments with average lengths of 1 and 1.5 kb in the presence of static

A-tract loops. The first of these samples, referred to as *1.5kbAtract*, contained the same 1.2 and 1.8 kb fragments of *1.5kbDNA*, except that a static A-tract loop was attached to the end of the 1.8 kb fragment (Figure 1). The condensation of *1.5kbAtract* produced relative rod populations at 2 min and at equilibrium that were less than those of *1.5kbDNA* and, within experimental error, the same as those measured for *3kbAtract* (Figures 3 and 7B). These results demonstrate that static loops affect both the kinetics of condensate formation and the equilibrium populations of rods and toroids for DNA fragments around 1.5 kb in length, even when the static loop is attached to only one of the two fragments in the sample.

Two additional samples with A-tract loops and shorter DNA strands were also studied. These two samples contained the same linear DNA fragments lengths as those of the sample *1kbDNA* but with the addition of A-tract loops. In the first of these two samples, referred to as *1kbAtract*, the A-tract loop was attached to the end of the 1.2 kb fragment (Figure 1). In the second sample, referred to as *1kb_Atract*, the A-tract loop was separate from all three of the linear fragments (Figure 1). The 2 min relative rod and toroid populations of samples *1kbAtract* and *1kb_Atract* were essentially the same as those observed for *1kbDNA*, with rods accounting for 30% of all condensates (Figure 7). However, the relative rod populations of *1kbAtract* and *1kb_Atract* decreased to equilibrium values of 13% and 9%, respectively, within 31 min after the initiation of condensation. These relative rod populations at equilibrium are on average 17% lower than that observed for *1kbDNA* (Figure 6). These results clearly demonstrate that the A-tract loops of samples *1kbAtract* and *1kb_Atract* alter the thermodynamics of DNA condensation in favor of toroids. In contrast, the 2 min populations of *1kbAtract* and *1kb_Atract* are not significantly different from the 2 min populations observed for *1kbDNA*. Thus, the A-tract loops present in the *1kbAtract* and *1kb_Atract* samples do not appear to alter the nucleation stage of condensate formation. This result may be due to a lower probability for A-tract loops in these samples to form proto-toroids (having less attached linear DNA) during the initial stages of condensation.

Considerations on the Origins of the Relative Equilibrium Populations of Toroids and Rods. The most obvious difference between DNA condensed in toroids and rods is that the DNA within toroids is smoothly and continuously bent, whereas the DNA within rods contains abrupt bends that are separated by linear regions. The coexistence of rods and toroids and the similar dimensions of these two morphologies has long been appreciated as an indication that the energy required for the smooth bending of the DNA within toroids is roughly equal to the energy required for the abrupt bends in rods (*1*). However, the amount of bending required to form a rod versus that to form a toroid does not necessarily scale equally as DNA length is decreased. In the case of toroids, the total amount of DNA bending within a toroid of a given size is expected to be essentially the same regardless of the length of DNA strands that comprise the toroid. In the case of rods, however, the number of abrupt bends required to form a rod of a given size would be expected to decrease as DNA strand length decreases. That is, as DNA length decreases, the number of strand ends within a rod of a given size increases, which increases the probability that DNA strand ends will be located at one end of the rod. When more strand ends are located at the ends of a rod, fewer abrupt bends per unit length of DNA are required to form the rod. This simple model for the length-dependent difference in DNA bending energy for rods versus toroids potentially explains the observed increase in equilibrium rod populations with decreasing DNA strand length.

In the present study, we have demonstrated that the introduction of static A-tract loops into DNA samples with average strand lengths of 1 and 1.5 kb resulted in a substantial increase in the relative population of toroids at morphological equilibrium. Given that the static curvature of these A-tract loops is similar to that of the smaller (i.e., inner) loops of DNA within toroidal condensates (*31*, *38*), it stands to reason that smoothly bent A-tract loops enhance toroid stability by requiring less energy for DNA bending but do not necessarily decrease or increase the energy required for rod formation.

CONCLUSIONS

The results presented here demonstrate that both kinetic and thermodynamic factors can influence experimentally observed relative populations of DNA rods and toroids. The overrepresentation of rods at earlier times following the initiation of condensation provides the first direct experimental proof that rods enjoy a kinetic advantage during the nucleation phase of condensation. It has been appreciated for some time that greater relative rod populations are observed as DNA fragment length is decreased. The results presented here provide direct evidence that this shift in condensate morphology is primarily due to a change in the relative thermodynamic stability of rods with respect to toroids, rather than a change in the kinetics of condensate nucleation. The results obtained with DNA samples containing phased A-tract sequences demonstrate that static loops can increase the relative populations of toroids by both increasing the probability of toroid nucleation and by increasing the thermodynamic stability of toroids with respect to rods. Finally, the results presented here support a model for the interconversion of multimolecular DNA rods to toroids that takes place through the exchange of DNA with solution, which allows a redistribution of DNA into a relative population of rods and toroids that is determined by their relative thermodynamic stabilities.

ACKNOWLEDGMENT

We thank the Georgia Institute of Technology Electron Microscopy Center for the use of the JEOL-100C and Ms. Yolande Berta for technical assistance.

SUPPORTING INFORMATION AVAILABLE

Analyses of free DNA concentrations by differential centrifugation and CD and histograms of toroid diameter and thickness as a function of time for the low and higher ionic strength buffers. This material is available free of charge via the Internet at http://pubs.acs.org.

REFERENCES

1. Bloomfield, V. A. (1991) Condensation of DNA by multivalent cations: Considerations on mechanism, *Biopolymers 31*, 1471−1481.

2. Bloomfield, V. A. (1996) DNA condensation, *Curr. Opin. Struct. Biol. 6*, 334−341.
3. Hud, N. V., and Downing, K. H. (2001) Cryoelectron microscopy of lambda phage DNA condensates in vitreous ice: The fine structure of DNA toroids, *Proc. Natl. Acad. Sci. U.S.A. 98*, 14925−14930.
4. Hud, N. V., and Vilfan, I. D. (2005) Toroidal DNA condensates: Unraveling the fine structure and the role of nucleation in determining size, *Annu. Rev. Biophys. Biomol. Struct. 34*, 295−318.
5. Haynes, M., Garrett, R. A., and Gratzer, W. B. (1970) Structure of nucleic acid-poly base complexes, *Biochemistry 9*, 4410−4416.
6. Evdokimov, Y. M., Platonov, A. L., Tikhonenko, A. S., and Varshavsky, Y. M. (1972) Compact form of double-stranded DNA in solution, *FEBS Lett. 23*, 180−184.
7. Gosule, L. C., and Schellman, J. A. (1976) Compact form of DNA induced by spermidine, *Nature 259*, 333−335.
8. Allison, S. A., Herr, J. C., and Schurr, J. M. (1981) Structure of viral Psi-29 DNA condensed by simple triamines: A light-scattering and electron-microscopy study, *Biopolymers 20*, 469−488.
9. Post, C. B., and Zimm, B. H. (1982) Theory of DNA condensation: Collapse versus aggregation, *Biopolymers 21*, 2123−2137.
10. Hud, N. V., Allen, M. J., Downing, K. H., Lee, J., and Balhorn, R. (1993) Identification of the elemental packing unit of DNA in mammalian sperm cells by atomic-force microscopy, *Biochem. Biophys. Res. Commun. 193*, 1347−1354.
11. Yoshikawa, K., and Matsuzawa, Y. (1996) Nucleation and growth in single DNA molecules, *J. Am. Chem. Soc. 118*, 929−930.
12. Bloomfield, V. A. (1997) DNA condensation by multivalent cations, *Biopolymers 44*, 269−282.
13. Balhorn, R., Cosman, M., Thornton, K., Krishnan, V. V., Corzett, M., Bench, G., Kramer, C., Lee, J., IV, Hud, N. V., Allen, M., Prieto, M., Meyer-Ilse, W., Brown, J. T., Kirz, J., Zhang, X., Bradbury, E. M., Maki, G., Braun, R. E., and Breed, W. (1999) in *The Male Gamete: From Basic Knowledge to Clinical Applications* (Gagnon, C., Ed.) pp 55−70, Cache River Press, Vienna, IL.
14. Lambert, O., Letellier, L., Gelbart, W. M., and Rigaud, J. L. (2000) DNA delivery by phage as a strategy for encapsulating toroidal condensates of arbitrary size into liposomes, *Proc. Natl. Acad. Sci. U.S.A. 97*, 7248−7253.
15. Vilfan, I. D., Conwell, C. C., and Hud, N. V. (2004) Formation of native-like mammalian sperm cell chromatin with folded bull protamine, *J. Biol. Chem. 279*, 20088−20095.
16. Lerman, L. S. (1971) Transition to a compact form of DNA in polymer solutions, *Proc. Natl. Acad. Sci. U.S.A. 68*, 1886−1890.
17. Oosawa, F. (1971) *Polyelectrolytes*, Marcel Dekker, New York.
18. Manning, G. S. (1977) Limiting laws and counterion condensation in polyelectrolyte solutions. 4. Approach to limit and extraordinary stability of charge fraction, *Biophys. Chem. 7*, 95−102.
19. Manning, G. S. (1978) Limiting laws and counterion condensation in polyelectrolyte solutions. 5. Further development of chemical-model, *Biophys. Chem. 9*, 65−70.
20. Ubbink, J., and Odijk, T. (1995) Polymer-induced and salt-induced toroids of hexagonal DNA, *Biophys. J. 68*, 54−61.
21. Takahashi, M., Yoshikawa, K., Vasilevskaya, V. V., and Khokhlov, A. R. (1997) Discrete coil-globule transition of single duplex DNAs induced by polyamines, *J. Phys. Chem. B 101*, 9396−9401.
22. Park, S. Y., Harries, D., and Gelbart, W. M. (1998) Topological defects and the optimum size of DNA condensates, *Biophys. J. 75*, 714−720.
23. Ha, B. Y., and Liu, A. J. (1999) Kinetics of bundle growth in DNA condensation, *Europhys. Lett. 46*, 624−630.
24. Ivanov, V. A., Stukan, M. R., Vasilevskaya, V. V., Paul, W., and Binder, K. (2000) Structures of stiff macromolecules of finite chain length near the coil-globule transition: A Monte Carlo simulation, *Macromol. Theory Simul. 9*, 488−499.
25. Sakaue, T., and Yoshikawa, K. (2002) Folding/unfolding kinetics on a semiflexible polymer chain, *J. Chem. Phys. 117*, 6323−6330.
26. Montesi, A., Pasquali, M., and MacKintosh, F. C. (2004) Collapse of a semiflexible polymer in poor solvent, *Phys. Rev. E: Stat. Phys., Plasmas, Fluids, Relat. Interdiscip. Top. 69*, 021916-1−021916-10.
27. Mahato, R. I., Takakura, Y., and Hashida, M. (1997) Nonviral vectors for *in vivo* gene delivery: Physicochemical and pharmacokinetic considerations, *Crit. Rev. Ther. Drug Carrier Syst. 14*, 133−172.
28. Rolland, A. (1998) From genes to gene medicines: recent advances in nonviral gene delivery, *Crit. Rev. Ther. Drug Carrier Syst. 15*, 143−198.
29. Arscott, P., Ma, C., Wenner, J., and Bloomfield, V. (1995) DNA condensation by cobalt hexaammine(III) in alcohol-water mixtures: Dielectric constant and other solvent effects, *Biopolymers 36*, 345−364.
30. Conwell, C. C., and Hud, N. V. (2004) Evidence that both kinetic and thermodynamic factors govern DNA toroid dimensions: Effects of magnesium(II) on DNA condensation by hexammine cobalt(III), *Biochemistry 43*, 5380−5387.
31. Conwell, C. C., Vilfan, I. D., and Hud, N. V. (2003) Controlling the size of nanoscale toroidal DNA condensates with static curvature and ionic strength, *Proc. Natl. Acad. Sci. U.S.A. 100*, 9296−9301.
32. Marquet, R., Wyart, A., and Houssier, C. (1987) Influence of DNA length on spermine-induced condensation: Importance of the bending and stiffening of DNA, *Biochim. Biophys. Acta 909*, 165−172.
33. Arscott, P. G., Li, A. Z., and Bloomfield, V. A. (1990) Condensation of DNA by trivalent cations. 1. Effects of DNA length and topology on the size and shape of condensed particles, *Biopolymers 30*, 619−630.
34. Sarkar, T., Conwell, C. C., Harvey, L. C., Santai, C. T., and Hud, N. V. (2005) Condensation of oligonucleotides assembled into nicked and gapped duplexes: potential structures for oligonucleotide delivery, *Nucleic Acids Res. 33*, 143−151.
35. Plum, G. E., Arscott, P. G., and Bloomfield, V. A. (1990) Condensation of DNA by trivalent cations. 2. Effects of cation structure, *Biopolymers 30*, 631−643.
36. Vijayanathan, V., Thomas, T., Shirahata, A., and Thomas, T. J. (2001) DNA condensation by polyamines: A laser light scattering study of structural effects, *Biochemistry 40*, 13644−13651.
37. Hud, N. V., Downing, K. H., and Balhorn, R. (1995) A constant radius of curvature model for the organization of DNA in toroidal condensates, *Proc. Natl. Acad. Sci. U.S.A. 92*, 3581−3585.
38. Shen, M. R., Downing, K. H., Balhorn, R., and Hud, N. V. (2000) Nucleation of DNA condensation by static loops: Formation of DNA toroids with reduced dimensions, *J. Am. Chem. Soc. 122*, 4833−4834.
39. Su, T. J., Theofanidou, E., Arlt, J., Dryden, D. T. F., and Crain, J. (2004) Single molecule fluorescence imaging and its application to the study of DNA condensation, *J. Fluoresc. 14*, 65−69.
40. Noguchi, H., and Yoshikawa, K. (2000) Folding path in a semiflexible homopolymer chain: A Brownian dynamics simulation, *J. Chem. Phys. 113*, 854−862.
41. Schnurr, B., MacKintosh, F. C., and Williams, D. R. M. (2000) Dynamical intermediates in the collapse of semiflexible polymers in poor solvents, *Europhys. Lett. 51*, 279−285.
42. Stevens, M. J. (2001) Simple simulations of DNA condensation, *Biophys. J. 80*, 130−139.
43. Schnurr, B., Gittes, F., and MacKintosh, F. C. (2002) Metastable intermediates in the condensation of semiflexible polymers, *Phys. Rev. E: Stat. Phys., Plasmas, Fluids, Relat. Interdiscip. Top. 65*, 061904-1−061904-13.
44. Ou, Z., and Muthukumar, M. (2005) Langevin dynamics of semiflexible polyelectrolytes: Rod-toroid-globule-coil structures and counterion distribution, *J. Chem. Phys. 123*, 074905-1−074905-9.
45. Nguyen, T. T., and Shklovskii, B. I. (2002) Kinetics of macroion coagulation induced by multivalent counterions, *Phys. Rev. E: Stat. Phys., Plasmas, Fluids, Relat. Interdiscip. Top. 65*, 031409-1−031409-7.
46. He, S. Q., Arscott, P. G., and Bloomfield, V. A. (2000) Condensation of DNA by multivalent cations: Experiment studies of condensation kinetics, *Biopolymers 53*, 329−341.
47. Huey, R., and Mohr, S. C. (1981) Condensed states of nucleic acids. III. Psi(+) and Psi(−) conformational transitions of DNA induced by ethanol and salt, *Biopolymers 20*, 2533−2552.
48. Arscott, P. G., Ma, C. L., Wenner, J. R., and Bloomfield, V. A. (1995) DNA condensation by cobalt hexaammine(III) in alcohol-water mixtures: Dielectric constant and other solvent effects, *Biopolymers 36*, 345−364.
49. Schnell, J. R., Berman, J., and Bloomfield, V. A. (1998) Insertion of telomere repeat sequence decreases plasmid DNA condensation by cobalt (III) hexaammine, *Biophys. J. 74*, 1484−1491.

50. Deng, H., and Bloomfield, V. A. (1999) Structural effects of cobalt-amine compounds on DNA condensation, *Biophys. J. 77*, 1556−1561.
51. Vasilevskaya, V. V., Khokhlov, A. R., Kidoaki, S., and Yoshikawa, K. (1997) Structure of collapsed persistent macromolecule: Toroid vs spherical globule, *Biopolymers 41*, 51−60.
52. Doye, J. P. K., Sear, R. P., and Frenkel, D. (1998) The effect of chain stiffness on the phase behaviour of isolated homopolymers, *J. Chem. Phys. 108*, 2134−2142.
53. Kolinski, A., Skolnick, J., and Yaris, R. (1986) The collapse transition of semiflexible polymers. A Monte Carlo simulation of a model system, *J. Chem. Phys. 85*, 3585−3597.
54. Kuznetsov, Y. A., Timoshenko, E. G., and Dawson, K. A. (1996) Equilibrium and kinetic phenomena in a stiff homopolymer and possible applications to DNA, *J. Chem. Phys. 105*, 7116−7134.
55. Noguchi, H., and Yoshikawa, K. (1998) Morphological variation in a collapsed single homopolymer chain, *J. Chem. Phys. 109*, 5070−5077.
56. Kuznetsov, Y. A., and Timoshenko, E. G. (1999) On the conformational structure of a stiff homopolymer, *J. Chem. Phys. 111*, 3744−3752.
57. Chattoraj, D. K., Gosule, L. C., and Schellman, J. A. (1978) DNA condensation with polyamines. II. Electron microscopic studies, *J. Mol. Biol. 121*, 327−337.
58. Eickbush, T., and Moudrianakis, E. (1978) The compaction of DNA helices into either continuous supercoils or folded-fiber rods and toroids, *Cell 13*, 295−306.
59. Porschke, D. (1984) Dynamics of DNA condensation, *Biochemistry 23*, 4821−4828.
60. Tecle, M., Preuss, M., and Miller, A. D. (2003) Kinetic study of DNA condensation by cationic peptides used in nonviral gene therapy: Analogy of DNA condensation to protein folding, *Biochemistry 42*, 10343−10347.
61. Widom, J., and Baldwin, R. L. (1983) Monomolecular condensation of lambda-DNA induced by cobalt hexammine, *Biopolymers 22*, 1595−1620.
62. Rivetti, C., Walker, C., and Bustamante, C. (1998) Polymer chain statistics and conformational analysis of DNA molecules with bends or sections of different flexibility, *J. Mol. Biol. 280*, 41−59.
63. Hud, N. V., and Plavec, J. (2003) A unified model for the origin of DNA sequence-directed curvature, *Biopolymers 69*, 144−159.
64. Reich, Z., Ghirlando, R., and Minsky, A. (1992) Nucleic acids packaging process: Effects of adenine tracts and sequence-dependent curvature, *J. Biomol. Struct. Dyn. 9*, 1097−1109.

BI060396C